Geophysical Research Letters

RESEARCH LETTER
10.1029/2020GL090296

Key Points:
- In the temperature anisotropic solar wind, a group of rotational discontinuities caused a substantial decrease in the dynamic pressure
- Along with the magnetospheric relaxation within 200 s, the storm-injected protons experienced betatron and Fermi decelerations
- The adiabatical reduction of hot proton fluxes suppressed the EMIC wave instabilities in the inner magnetosphere

Supporting Information:
- Supporting Information S1

Correspondence to:
Z. Su,
szpe@mail.ustc.edu.cn

Citation:
Liu, N., Su, Z., Gao, Z., Zheng, H., Wang, Y., & Wang, S. (2020). Can solar wind decompressive discontinuities suppress magnetospheric electromagnetic ion cyclotron waves associated with fresh proton injections? *Geophysical Research Letters*, *47*, e2020GL090296. https://doi.org/10.1029/2020GL090296

Received 12 AUG 2020
Accepted 21 AUG 2020
Accepted article online 25 AUG 2020

Can Solar Wind Decompressive Discontinuities Suppress Magnetospheric Electromagnetic Ion Cyclotron Waves Associated With Fresh Proton Injections?

Nigang Liu[1,2,3], Zhenpeng Su[1,2], Zhonglei Gao[4,5], Huinan Zheng[1,2], Yuming Wang[1,2], and Shui Wang[1,2]

[1]CAS Key Laboratory of Geospace Environment, Department of Geophysics and Planetary Sciences, University of Science and Technology of China, Hefei, China, [2]CAS Center for Excellence in Comparative Planetology, University of Science and Technology of China, Hefei, China, [3]Anhui Mengcheng Geophysics National Observation and Research Station, University of Science and Technology of China, Mengcheng, China, [4]Institute of Space Science and Applied Technology, Harbin Institute of Technology, Shenzhen, China, [5]School of Physics and Electronic Sciences, Changsha University of Science and Technology, Changsha, China

Abstract Electromagnetic ion cyclotron (EMIC) waves play an important role in the energy transfer among particles of different energies and species in the magnetosphere, whose drivers have been commonly recognized as solar wind compressions and storm/substorm proton injections. However, how the solar wind decompressions related to frequently occurring discontinuities compete with the proton injections in the evolution of EMIC waves has been rarely investigated. Here we present a complete end-to-end observation by Wind, THEMIS, and Van Allen Probes missions during the main phase of the 23 February 2014 storm of a succession of solar wind rotational discontinuities decompressing the magnetosphere within 200 s, adiabatically decelerating the freshly injected >10 keV protons, and thus suppressing the EMIC waves in the inner magnetosphere. Our results highlight the importance of solar wind conditions for the evolution of inner magnetospheric EMIC waves from a new perspective.

Plain Language Summary Magnetospheric electromagnetic ion cyclotron (EMIC) waves are ultralow-frequency (0.1–5.0 Hz) pulsations observable both on the ground and in space. They contribute significantly to the magnetospheric particle dynamics and the magnetosphere-ionosphere coupling. Previous studies have recognized two main drivers for EMIC waves: solar wind compressions and magnetospheric storm/substorm proton injections. However, both compressive and decompressive discontinuities, with dynamic pressure jumps on a timescale of seconds to minutes, can occur in the solar wind upstream of Earth, and under the condition of the fresh proton injections, to what extent the solar wind decompressive discontinuities can affect the EMIC waves in the inner magnetosphere remains to be determined. On the basis of observations by three space missions in the solar wind and magnetosphere during the main phase of a moderate storm, we show that the solar wind decompressive discontinuities can cause a relaxation of the magnetosphere, deceleration of the freshly injected protons, and thus quenching of the EMIC waves in the inner magnetosphere. These results illustrate the importance of solar wind conditions for the evolution of inner magnetospheric EMIC waves from a new perspective.

1. Introduction

In the terrestrial magnetosphere, electromagnetic ion cyclotron (EMIC) waves contribute significantly to the precipitation of energetic particles (Albert & Bortnik, 2009; Bortnik et al., 2006; Denton et al., 2019; Jordanova et al., 2008; Li et al., 2007; Lyons & Thorne, 1972; Omura & Zhao, 2012; Shprits et al., 2016; Summers & Thorne, 2003; Su et al., 2011; Thorne & Kennel, 1971; Usanova et al., 2014) and the heating of suprathermal particles (Bortnik et al., 2010; Thorne & Horne, 1992, 1994; Yuan et al., 2014; Zhou et al., 2013). EMIC waves are ultralow-frequency Pc1–2 (0.1–5.0 Hz) pulsations observable both on the ground (Harang, 1936; Sucksdorff, 1936) and in space (Erlandson et al., 1992; Fraser et al., 2010; Perraut, 1982). These waves are separated into hydrogen, helium, and oxygen bands by the corresponding ion gyrofrequencies in the frequency-time spectrogram (Anderson et al., 1990; Bossen et al., 1976; Fraser & McPherron, 1982; Pickett et al., 2010). They arise from the linear or nonlinear instabilities of hot protons

with a sufficiently strong temperature anisotropy (Chen et al., 2010; Cornwall, 1965; Horne & Thorne, 1993; Nakamura et al., 2016; Omura et al., 2010; Zhang et al., 2014). Their source regions are close to the equator in the inner magnetosphere (Anderson et al., 1992; Fraser et al., 2010; Halford et al., 2015; Loto'Aniu et al., 2005; Wang et al., 2015) and could extend to midlatitudes in the outer magnetosphere (Jun et al., 2019; Usanova et al., 2012).

There have been proposed two classes of drivers for EMIC waves: (1) magnetospheric storm and substorm proton injections (Cornwall et al., 1970; Halford et al., 2016; Jordanova et al., 2001; Remya et al., 2018) and (2) solar wind compressions (Engebretson et al., 2002; Hirasawa, 1981; Kangas et al., 1986; Troitskaya, 1967; Usanova et al., 2008). For the former, the freshly injected protons are expected to have a strong temperature anisotropy and provide abundant free energy not only on the nightside but also on the dayside (Fraser et al., 2013; Remya et al., 2020; Zhang et al., 2016). For the latter, the compressed magnetosphere is envisioned to favor the buildup of the temperature anisotropy of preexisting protons through adiabatic acceleration (Olson & Lee, 1983), drift shell splitting (Sibeck et al., 1987), or drift orbit bifurcation (McCollough et al., 2012). In fact, the storm and substorm activities are often triggered by the coronal mass ejections (CMEs) and corotating interaction regions (CIRs) in the solar wind. These solar wind structures consist of numerous discontinuities with significant pressure jumps (Dalin et al., 2002; Neugebauer, 2006; Riazantseva et al., 2007; Wu et al., 1993; Zuo et al., 2015). However, in contrast to the influence of solar wind compressions (Anderson & Hamilton, 1993; Cho et al., 2017; Engebretson et al., 2002; McCollough et al., 2009; Saikin et al., 2016; Usanova et al., 2008), the competition between solar wind decompressions and fresh proton injections in the evolution of EMIC waves has received much less attention.

In this letter, on the basis of observations from Wind (Ogilvie & Desch, 1997), Time History of Events and Macroscale Interactions during Substorm (THEMIS) (Angelopoulos, 2008), and Van Allen Probes (Mauk et al., 2013) missions, we show that the solar wind decompressions of rotational discontinuities can cause betatron and Fermi decelerations of the freshly injected protons and then suppress EMIC waves in the inner magnetosphere.

2. Instrument and Data

We use the Wind, THEMIS, and Van Allen Probes missions to understand the interplanetary and magnetospheric processes regarding the evolution of EMIC waves. The Wind spacecraft was operating in a halo orbit around the Lagrange point L1 (over 200 R_E away from Earth). We use the solar wind data from the Magnetic Field Investigation (MFI Koval & Szabo, 2013), the Solar Wind Experiment (SWE Ogilvie et al., 1995), and the 3-D Plasma and Particle Investigation (3DP Lin et al., 1995) onboard WIND satellite. The THEMIS mission consisted of five satellites, and three (TH-A, TH-D, and TH-E) of them were operating in highly elliptical orbits with apogees around 10 R_E away from Earth. We use only the data from the Electrostatic Analyzer (ESA McFadden et al., 2008), the Solid State Telescope (SST Angelopoulos, 2008), the Electric Field Instrument (EFI Bonnell et al., 2008), and the Fluxgate Magnetometer (FGM Auster et al., 2008) onboard the TH-D satellite. The Van Allen Probes mission contains two identically instrumented probes operating in highly elliptical orbits with apogees about 6 R_E. We use the data from the Electric and Magnetic Field Instrument and Integrated Science suite (EMFISIS Kletzing et al., 2013), the Electric Field and Wave instrument (EFW Wygant et al., 2013), and the Helium Oxygen Proton Electron Mass Spectrometer (HOPE Funsten et al., 2013) of the Energetic particle, Composition and the Thermal plasma suite (ECT Spence et al., 2013), and the Radiation Belt Storm Probes Ion Composition Experiment (RBSPICE Mitchell et al., 2013) onboard the Van Allen Probes mission. Using the Fourier transform of the local electromagnetic fields from the TH-D satellite and the Van Allen Probes, we obtain the electromagnetic spectral matrices of magnetospheric EMIC waves. Utilizing the singular value decomposition technique to the obtained spectral matrices, we can estimate the propagation and polarization characteristics of waves (Santolík et al., 2002, 2003). From the cross-power spectra between components of the electric and magnetic fields, we can determine the wave Poynting fluxes (Santolík et al., 2010). We infer the local electron densities from the potential (Li et al., 2010) of the TH-D satellite and from the upper hybrid frequency (Kurth et al., 2014) measured by the Van Allen Probes.

3. Event Overview

Figures 1a–1c display the solar wind parameters observed by Wind during 21–26 February 2014. The interaction between fast (580 km s^{-1}) and slow (430 km s^{-1}) streams formed a CIR with remarkable enhancements

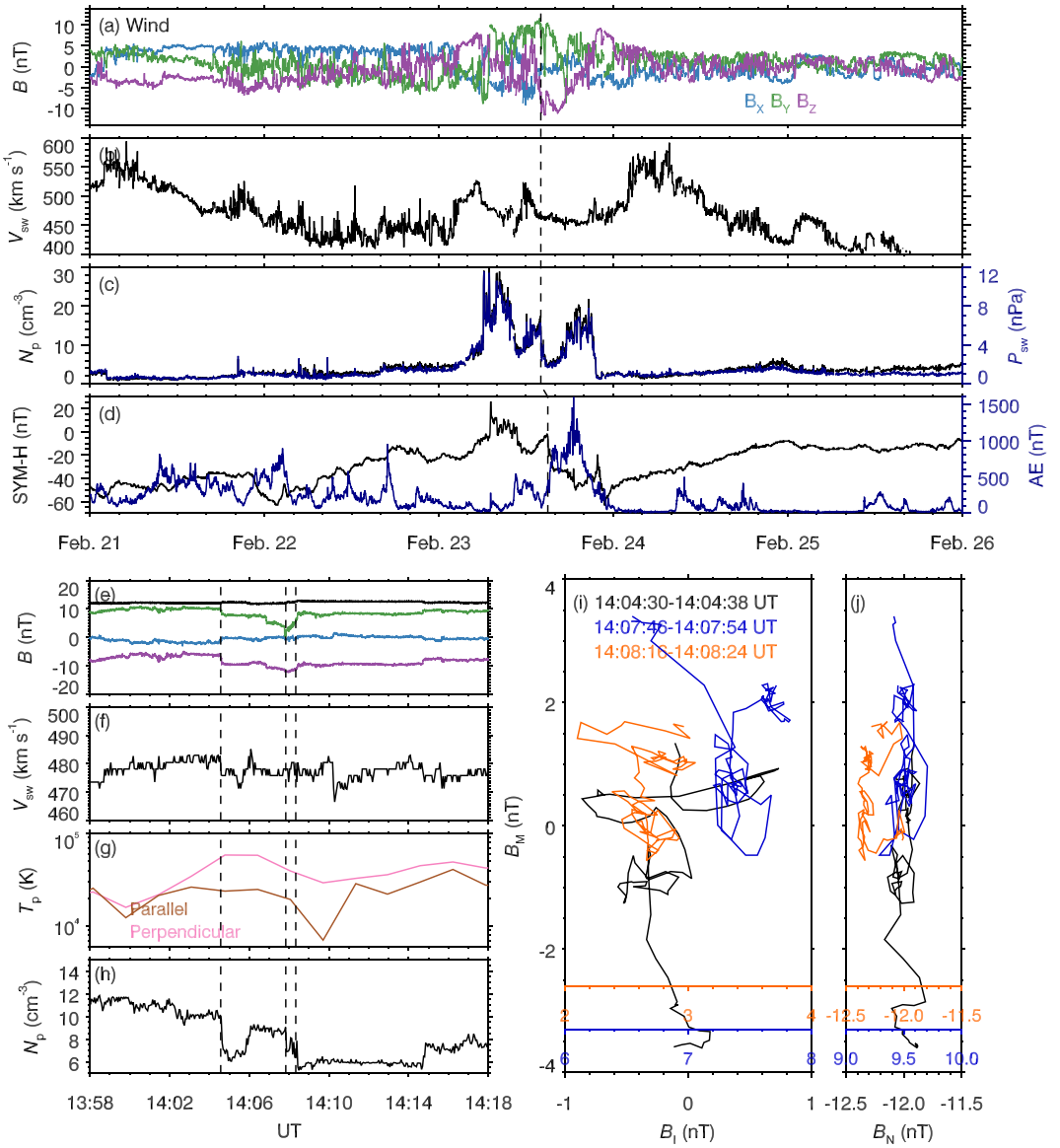

Figure 1. Solar wind properties observed by Wind and geomagnetic activities: (a, e) solar wind magnetic components (B_X, B_Y, B_Z) and strength B in the GSE coordinate system; (b, f) solar wind velocity V_{SW}; (c, h) solar wind proton density N_p and dynamic pressure P_{SW}; (d) geomagnetic indices SYM-H and AE; (g) parallel $T_{p\parallel}$ and perpendicular $T_{p\perp}$ temperatures of solar wind protons; and (i, j) solar wind magnetic normal B_N, intermediately varying B_I, and maximally varying B_M components in the minimum variance coordinate systems during three time periods. Figures 1a–1d provide a large-scale view from 21 February 2014 to 26 February 2014, with the dashed line marking the solar wind decompression on 23 February 2014. Figures 1e–1h give a zoom-in view of the solar wind decompression, with the three dashed lines marking the rotational discontinuities. Figures 1i and 1j plot the magnetic fields adjacent to the three discontinuities in the minimum variance coordinate systems.

in both density and magnetic field magnitude (Gosling & Pizzo, 1999; Smith & Wolfe, 1976). As illustrated in Figure 1d, the CIR had triggered a moderate storm (with the SYM-H minimum of −50 nT) and the prolonged substorms (with the AE maximum of 1,500 nT) in the magnetosphere. Engebretson et al. (2015) have analyzed the EMIC waves associated with the solar wind compression during the initial phase of this storm. We here focus on the competition between the solar wind decompression and the proton injection in the generation of EMIC waves around 15:03 UT on 23 February 2014 during the main phase. The corresponding solar wind was sampled by Wind at approximately 1 hr earlier (Figures 1e–1h). From 13:58 to 14:18 UT, there were a series of discontinuities roughly conserving velocity and magnetic field magnitude but accompanied

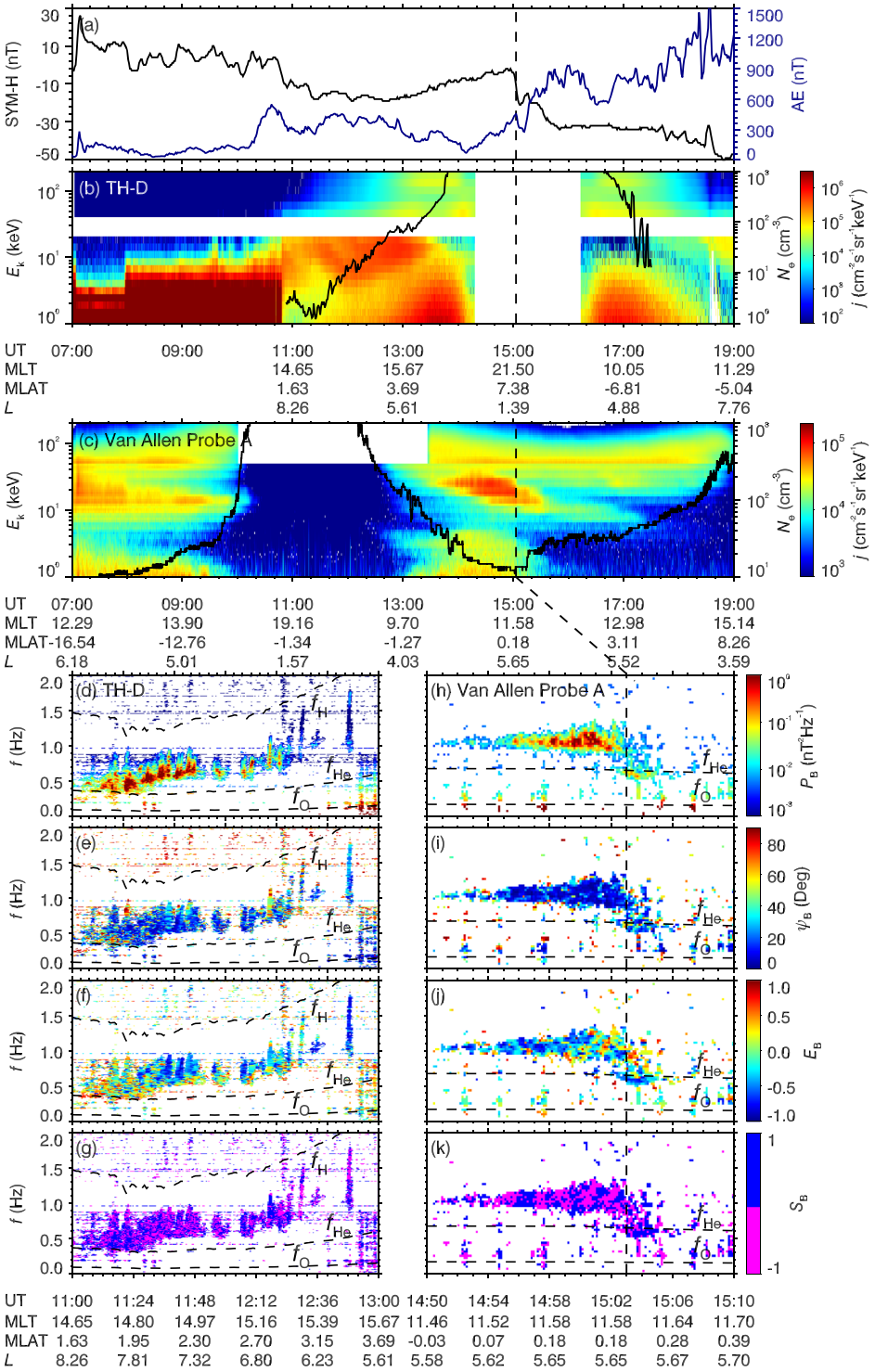

Figure 2. Magnetospheric protons and waves observed by TH-D and Van Allen Probe A during the initial and main phases of the 23 February 2014 storm: (a) geomagnetic indices SYM-H and AE; (b, c) hot proton flux j and background electron density N_e; (d, h) magnetic power P_B; (e, i) normal angle ψ_B; (f, j) elipticity E_B (negative for left-handed polarizations and positive for right-handed ones); and (g, k) field-aligned Poynting flux sign S_B (positive for parallel flowing and negative for antiparallel flowing) for EMIC waves. The vertical dashed lines mark the arrival of the solar wind decompressive discontinuities. In Figure 2b, the values of L, MLT, and MLAT are not listed for TH-D outside the magnetopause approximately before 10:50 UT. In Figure 2c, the >50 keV proton fluxes measured by RBSPICE have been reduced by a factor of 3 to match the HOPE data. In Figures 2d–2k, EMIC waves are separated by the ion gyrofrequencies f_H, f_{He}, and f_O (dashed lines).

by notable changes in density and magnetic field direction. For the three discontinuities with the most outstanding density jumps in the minimum variance coordinate systems (Sonnerup & Cahill, 1967), the normal magnetic field component was in dominance (70–85% of the total magnetic field strength), and the other components exhibited a rotation of polarity (Figures 1i and 1j). These results imply that a cluster of rotational discontinuities (Smith, 1973) collectively produced a considerable decompression of the solar wind and then a relaxation of the magnetosphere (characterized as a sudden decrease in the SYM-H index from −2 to −20 nT). In an isotropic plasma medium, the density and dynamic pressure should be continuous across the rotational discontinuity. However, the temperature anisotropic solar wind (Figure 1g) allowed changes in density and dynamic pressure across the rotational discontinuity (Dalin et al., 2002; Hudson, 1970, 1971, 1973; Neugebauer, 2006).

Figure 2 shows the observations of proton fluxes and EMIC waves during the initial and main phases of the 23 February 2014 storm. Around 10:00 UT, the decrease of SYM-H index and the increase of AE index manifested the onset of the main phase. In general, the hot protons originate from the nightside plasmasheet and under the action of both magnetic and electric fields, drift to the dayside on a timescale of hours (e.g., Fok et al., 1999). TH-D and Van Allen Probe A collectively sampled the afternoon and prenoon sectors, providing a global picture of dayside EMIC waves driven by the proton injection. Because of the energy dependence of drift velocity, the dayside injection appeared as an energy-dispersive enhancement in the energy-time spectrogram for both TH-D (after 11:20 UT in Figures 2b and S1c in the supporting information) and Van Allen Probe A (after 13:00 UT in Figures 2c and S1d). Specifically, as indicated by the comparison between the prenoon data during the main phase (14:00–15:00 UT) with those during the initial phase (04:00–05:00 UT) in Figure S1e, the injection had caused the 20.7 keV proton fluxes to increase by 5–10 times (dependent on the pitch angle and the L shell). Probably caused by drift-shell splitting, magnetopause shadowing or outward diffusive loss (Sibeck et al., 1987; Takahashi et al., 1997; Yue et al., 2017), the injected protons appeared as butterfly pitch-angle distributions at outer L shells (Figures S1e). In the afternoon sector (TH-D), there were hydrogen-band EMIC waves from just inside the magnetopause ($L = 8.3$) down to $L = 5.8$. In the prenoon sector (Van Allen Probe A), the corresponding hydrogen-band EMIC waves occurred in the frequency range of 0.9–1.5 Hz with an average wave amplitude of ∼0.5 nT, accompanied by some intermittent and weak helium-band EMIC waves. All these dayside EMIC waves were mainly left-handed polarized ($E_B < -0.2$) and propagated bidirectionally ($S_B = \pm 1$) with small normal angles ($\psi_B < 20°$), consistent with the theoretical prediction of the near-equatorially generated guided-mode waves (Rauch & Roux, 1982). Particularly for Van Allen Probe A, the EMIC wave Poynting fluxes changed directions alternately, similar to those equatorial EMIC waves reported by Loto'Aniu et al. (2005). The initial- and main-phase EMIC waves observed by Van Allen Probe A (Figures S1a and S1g) were quite different in solar-wind condition, occurrence location, and spectral characteristics. During the initial phase, the intense EMIC waves with rising tone structures (Figure 5 of Engebretson et al., 2015) occurred primarily outside $L = 5.7$ and were quenched when the solar wind dynamic pressure decreased from 12 to 6 nPa at 08:00 UT. In contrast, during the main phase with the solar wind dynamic pressure of about 5 nPa, the unstructured (Figure 2h) EMIC waves emerged inside $L = 5.67$. The proton injection was likely the dominant driver of these main-phase EMIC waves even though the solar wind dynamic pressure was not at an extremely low level. In response to the solar wind decompression at 15:03 UT, the hot proton fluxes decreased obviously, and the EMIC waves became quite weak or unobservable. These observations suggest that, even with the fresh injection of hot protons in the inner magnetosphere, the solar wind decompressive discontinuities could suppress the EMIC waves.

4. Physical Mechanisms

Figures 3a–3d give a zoom-in view of the wave evolution conditions around the solar wind decompression on 23 February 2014. Across the decompression, the cold electron density changed little, the magnetic magnitude decreased by 30 nT, and the proton fluxes particularly near $\alpha = 90°$ decreased by up to 30%. The decrease of hot proton fluxes was unfavorable to the growth of waves. On the contrary, the decrease of magnetic magnitude might promote the wave growth by reducing the minimum resonance energy E_{min} for protons (Summers et al., 2007). Here E_{min} is defined as

$$E_{min} = \frac{1}{2} m_H v_R^2, \quad (1)$$

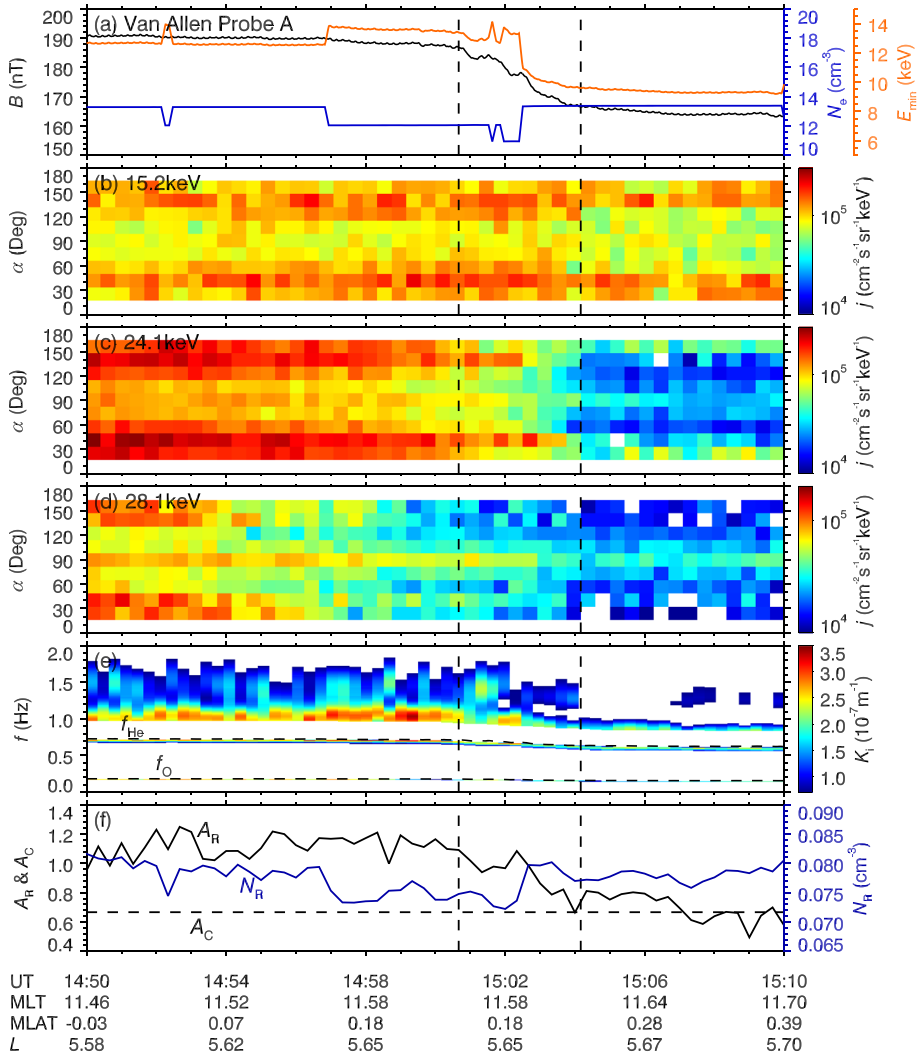

Figure 3. EMIC wave instabilities around the solar wind decompression: (a) background magnetic field B, density N_e, and minimum resonant energy E_{min} for EMIC wave at $0.4f_H \approx 1$ Hz (central frequency of the observed EMIC waves); (b–d) proton differential flux j at 15.2, 24.1, and 28.1 keV; (e) linear spatial growth rate K_i of parallel propagating EMIC waves, with the overplotted lines for ion gyrofrequencies f_{He} and f_O; (f) resonant proton anisotropy A_R (black solid line), anisotropy threshold A_C (black horizontal dashed line), and resonant proton density N_R (blue solid line) for EMIC wave at $0.4f_H$. The two vertical dashed lines denote the time period of the magnetic field relaxation.

with the resonant parallel velocity $v_R = \frac{\omega-\Omega_H}{k}$, angular gyrofrequency $\Omega_H = 2\pi f_H$ and rest mass m_H of protons, and the wave vector k and angular frequency ω. The protons with energies $>E_{min}$ can contribute to the growth of waves.

To determine the combined effect of different factors on the EMIC instabilities, we calculate the linear growth rates of parallel-propagating waves using our previously developed code (Liu et al., 2018a, 2018b; Su et al., 2018). The expressions for the spatial K_i and temporal γ growth rates can be written as (Chen et al., 2010; Kennel, 1966; Kennel & Petschek, 1966)

$$K_i = \gamma/|\mathbf{v}_g|, \tag{2}$$

$$\gamma = \frac{1}{\frac{\partial D}{\partial \omega}} \frac{4\pi e^2}{\epsilon_0 m_H} \frac{P(R-L)}{\omega^2} N_R \cdot \left(A_R - A_C\right), \tag{3}$$

$$N_R = 2\pi \frac{\Omega_H - \omega}{k} \cdot \int_0^\infty v_\perp dv_\perp F|_{v_\parallel = v_R}, \tag{4}$$

$$A_R = \frac{\int_0^\infty v_\perp dv_\perp \left(v_\parallel \frac{\partial F}{\partial v_\perp} - v_\perp \frac{\partial F}{\partial v_\parallel}\right) \frac{v_\perp}{v_\parallel}}{2\int_0^\infty v_\perp dv_\perp F}|_{v_\parallel = v_R}, \quad (5)$$

$$A_C = \frac{1}{(\Omega_H/\omega) - 1}, \quad (6)$$

where F is the proton phase space density as a function of perpendicular $v_\perp$ and parallel $v_\parallel$ velocities; N_R and A_R can be interpreted as some measures of number density and anisotropy of resonant protons; A_C is the anisotropy threshold for the wave growth; D is the cold-plasma dispersion relation function; n is the refractive index; v_g is the wave group velocity; L, R, and P are the standard Stix coefficients (Stix, 1962); and e and ε_0 are the elementary charge and vacuum permittivity.

The calculation of linear growth rates in our code requires the inputs of magnetic field magnitude, cold electron density, proton phase space density, and ion composition. The former two inputs are directly available from the observations. Using the smooth cubic spline approximation method, we have well modeled the observed evolution of the proton phase space density (Figure S2). The background cold (~ <1 eV) ions are normally hidden to the detector because of the repelling effect of the spacecraft potential in the magnetosphere (André & Cully, 2012; Sarno-Smith et al., 2016). Figures S3 and S4 show the ion densities estimated from the HOPE omnidirectional differential flux data (Equation A4, Goldstein et al., 2014) in different energy ranges. For this specific event, the spacecraft was charged to ~7 V (Figure S3), and the measurable ions were about 4% or less of the total ions (Figures 3a and S4a–S4c). Clearly, the abundance ratio of heavy ions tended to decrease with the energy decreasing (Figures S4d–S4f), and the available measurements were insufficient to determine the background cold ion compositions. Nevertheless, the available measurements of 7–100 eV implied the ion composition of >80% hydrogen, ~10% oxygen, and very limited helium. Considering the dominance of hydrogen-band EMIC waves (Figure 2h), we expediently set the cold ion compositions $\eta_H{:}\eta_{He}{:}\eta_O = 0.90{:}0.01{:}0.09$.

The obtained linear growth rates (Figure 3e) qualitatively explain the temporal evolution of EMIC waves observed by Van Allen Probe A. Before the decompression, the modeled hydrogen-band waves occur in the roughly same frequency range of 0.9–1.5 Hz as the observations, with a peak growth rate $K_i \sim 3.5\times10^{-7}\mathrm{m}^{-1}$. Because the growth of the helium- and oxygen-band waves is of a relatively low rate and limited to a very narrow frequency range, they seem to be difficult to cumulatively grow to the observable level. After the decompression, the modeled instability frequency range essentially narrows to 0.7–0.8 Hz, and the modeled growth rates mostly decrease to $1.0\times10^{-7}\mathrm{m}^{-1}$. As demonstrated in Figure 3f, the decompression has reduced the anisotropy A_R to a value quite close to or even below the threshold A_c, in contrast to a slight (~6%) increase in the number density of resonant protons N_R. For this specific event, the decrease of proton anisotropy is largely responsible for the quenching of EMIC waves. In addition, the change of the background magnetic field configuration might contribute, more or less, to the weakening of EMIC waves. The solar wind decompression can cause a relaxation of the magnetosphere and increase the background magnetic field inhomogeneity. In a more inhomogeneous magnetic field, the waves become easier to propagate obliquely and then have a lower integrated gain (Khazanov et al., 2006). The enhanced inhomogeneity enlarges the magnetic mirror force on resonant protons and then reduces the nonlinear growth rates of EMIC waves (Nakamura et al., 2016; Omura et al., 2010), analogous to the situation of whistler mode chorus waves (Liu et al., 2017).

In response to the solar wind decompression, the geomagnetic field changed within a time period of ~200 s (Figure 3a). For the resonant protons >10 keV (Figure 3a), their cyclotron, bounce, and drift periods were on the order of seconds, minutes, and hours, respectively. Hence, during the relaxation of the magnetosphere, the resonant protons conserved the first and second adiabatic invariants and experienced betatron and Fermi decelerations. The Liouville's theorem states that the adiabatic process does not change the phase space density in the adiabatic invariant space. Ignoring the drift process, we can estimate the adiabatic changes in the pitch angles, energies, and fluxes of hot protons (Figure 4). In the TA15 geomagnetic field model (Tsyganenko & Andreeva, 2015), Van Allen Probe A is around a magnetic field line with the foot point of $\lambda_{fp} = 66.8$ magnetic latitude at the predecompression time (14:55 UT). After the decompression, Van Allen Probe A passes the magnetic field line with nearly the same λ_{fp} at 15:10 UT. The most significant adiabatic deceleration occurs near $\alpha = 90°$ (Figure 4b), consistent with the observations (Figures 3b–3d).

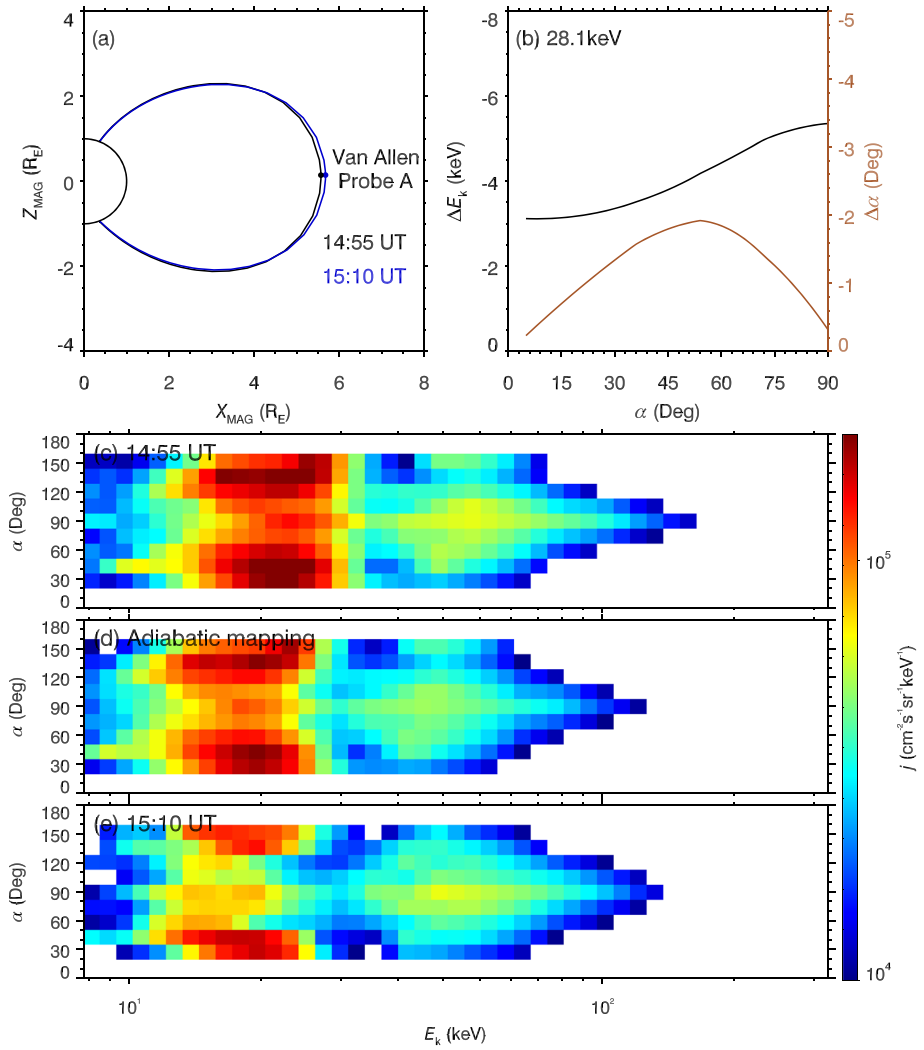

Figure 4. Adiabatic evolution of hot protons: (a) geomagnetic field lines with the same foot points at two different times in the meridian plane of the geomagnetic coordinate system, with two dots marking the corresponding locations of Van Allen Probe A; (b) adiabatic changes in energy ΔE_k and pitch angle $\Delta\alpha$ for the 21.8 keV protons; (c, e) proton differential flux j observed by Van Allen Probe A at 14:55 and 15:10 UT; and (d) proton differential flux j mapped adiabatically from 14:55 to 15:10 UT.

Slightly below 30 keV, because of the strong negative gradient of the predecompression phase space density with respect to energy, the adiabatic dropout of proton fluxes is the most prominent (Figures 3c and 3d). On the contrary, the weak gradient leads to a minor variation of proton fluxes near 15 keV (Figure 3b). These calculations support that the adiabatic betatron and Fermi deceleration processes over several bounce periods were largely responsible for the observed evolution of hot protons.

5. Summary

Previous studies have recognized two main drivers for EMIC waves: solar wind compressions and proton injections. Along with proton injections during storms and substorms, both solar wind compressions and decompressions related to the discontinuities on a timescale of seconds to minutes are likely to occur upstream of Earth. In contrast to previous studies, we focus on a rarely investigated aspect of the evolution of EMIC waves, that is, the competition between the solar wind decompressions and the proton injections. The new findings are summarized as follows:

1. The solar wind decompression can prevail over the proton injection in the evolution of magnetospheric EMIC waves during the storm main phase. In contrast to previous studies by observations or modeling

alone regarding the solar wind condition for the EMIC waves (e.g., Chen et al., 2014; Cho et al., 2017; Engebretson et al., 2015; Li et al., 2016; McCollough et al., 2009; Usanova et al., 2008), we present here both the multispacecraft observations and the data-driven modeling to demonstrate the complete physical chain for the competition between the solar wind decompression and the proton injection on 23 February 2014. Specifically, a 60% reduction of the solar wind dynamic pressure caused the relaxation of the magnetosphere within 200 s, diminished the anisotropy of the freshly injected protons by betatron and Fermi decelerations, and eventually resulted in the quenching of EMIC waves.

2. The rotational discontinuities in the temperature anisotropic solar wind can become effective in affecting the magnetospheric EMIC waves. Except for interplanetary shocks (e.g., Cattell et al., 2017; Engebretson et al., 2015; Lee, 2017; Zhang et al., 2008), other solar wind discontinuous structures including rotational, tangential, and contact discontinuities (Artemyev et al., 2019; Landau & Lifshitz, 1984) were rarely identified as the cause of variation in magnetospheric EMIC waves in previous studies. The contact discontinuities would rapidly decay into smooth transitions in the interplanetary space (Colburn & Sonett, 1966). The shocks and tangential discontinuities normally allow the abrupt variations in the dynamic pressure. For the rotational discontinuities, the dynamic pressure is continuous in an isotropic medium but could be discontinuous in a temperature anisotropic medium (Hudson, 1970). We present here the first report linking the magnetospheric EMIC wave quenching to the solar-wind rotational discontinuities.

Data Availability Statement

Van Allen Probes data were obtained online (from the websites: http://emfisis.physics.uiowa. edu/Flight/ for EMFSIS, http://www.space.umn.edu/rbspefw-data/ for EFW, http://www.rbsp-ect.lanl.gov/data_pub/ for ECT, and http://rbspice.ftecs.com/Data.html for RBSPICE. THEMIS data were obtained from an index online (website: http://themis.ssl.berkeley.edu/data/themis/). WIND data were obtained from the NASA website (https://wind.nasa.gov/data.php). Geomagnetic indices are obtained online (from the website: http://wdc.kugi.kyoto-u.ac.jp).

Acknowledgments
We acknowledge the entire Van Allen Probes, THEMIS, and WIND teams for the use of data. This work was supported by the Strategic Priority Research Program of Chinese Academy of Sciences Grant XDB 41000000, the National Natural Science Foundation of China Grants 41774170 and 41631071, the Chinese Academy of Sciences Grants KZCX2-EW-QN510 and KZZD-EW-01-4, the CAS Key Research Program of Frontier Sciences Grant QYZDB-SSW-DQC015, the National Key Basic Research Special Foundation of China Grant 2011CB811403, the National Postdoctoral Program for Innovative Talents Grant BX20190310, the China Postdoctoral Science Foundation Grant 2019M662171, and the Fundamental Research Funds for the Central Universities WK2080000005.

References

Albert, J. M., & Bortnik, J. (2009). Nonlinear interaction of radiation belt electrons with electromagnetic ion cyclotron waves. *Geophysical Research Letters*, *36*, L12110. https://doi.org/10.1029/2009GL038904

Anderson, B. J., Engebretson, M. J., Rounds, S. P., Zanetti, L. J., & Potemra, T. A. (1990). A statistical study of Pc3–5 pulsations observed by the AMPTE/CCE magnetic fields experiment. I—Occurrence distributions. *Journal of Geophysical Research*, *95*, 10,495–10,523. https://doi.org/10.1029/JA095iA07p10495

Anderson, B. J., Erlandson, R. E., & Zanetti, L. J. (1992). A statistical study of Pc 1–2 magnetic pulsations in the equatorial magnetosphere: 2. Wave properties. *Journal of Geophysical Research*, *97*, 3089.

Anderson, B. J., & Hamilton, D. C. (1993). Electromagnetic ion cyclotron waves stimulated by modest magnetospheric compressions. *Journal of Geophysical Research*, *98*, 11. https://doi.org/10.1029/93JA00605

André, M., & Cully, C. M. (2012). Low-energy ions: A previously hidden solar system particle population. *Geophysical Research Letters*, *39*, L03101. https://doi.org/10.1029/2011GL050242

Angelopoulos, V. (2008). The THEMIS mission. *Space Science Reviews*, *141*, 5–34. https://doi.org/10.1007/s11214-008-9336-1

Artemyev, A. V., Angelopoulos, V., Vasko, I. Y., Runov, A., Avanov, L. A., Giles, B. L., & Strangeway, R. J. (2019). On the kinetic nature of solar wind discontinuities. *Geophysical Research Letters*, *46*, 1185–1194. https://doi.org/10.1029/2018GL079906

Auster, H. U., Glassmeier, K. H., Magnes, W., Aydogar, O., Baumjohann, W., Constantinescu, D., et al. (2008). The THEMIS fluxgate magnetometer. *Space Science Reviews*, *141*, 235–264. https://doi.org/10.1007/s11214-008-9365-9

Bonnell, J. W., Mozer, F. S., Delory, G. T., Hull, A. J., Ergun, R. E., Cully, C. M., et al. (2008). The electric field instrument (EFI) for THEMIS. *Space Science Reviews*, *141*, 303–341. https://doi.org/10.1007/s11214-008-9469-2

Bortnik, J., Thorne, R. M., O'Brien, T. P., Green, J. C., Strangeway, R. J., Shprits, Y. Y., & Baker, D. N. (2006). Observation of two distinct, rapid loss mechanisms during the 20 November 2003 radiation belt dropout event. *Journal of Geophysical Research*, *111*, A12216. https://doi.org/10.1029/2006JA011802

Bortnik, J., Thorne, R. M., & Omidi, N. (2010). Nonlinear evolution of EMIC waves in a uniform magnetic field: 2. Test-particle scattering. *Journal of Geophysical Research*, *115*, A12242. https://doi.org/10.1029/2010JA015603

Bossen, M., McPherron, R. L., & Russell, C. T. (1976). A statistical study of PC1 magnetic pulsations at synchronous orbit. *Journal of Geophysical Research*, *81*(A34), 6083–6091. https://doi.org/10.1029/JA081i034p06083

Cattell, C., Breneman, A., Colpitts, C., Dombeck, J., Thaller, S., Tian, S., et al. (2017). Dayside response of the magnetosphere to a small shock compression: Van Allen Probes, Magnetospheric MultiScale, and GOES-13. *Geophysical Research Letters*, *44*, 8712–8720. https://doi.org/10.1002/2017GL074895

Chen, L., Jordanova, V. K., Spasojević, M., Thorne, R. M., & Horne, R. B. (2014). Electromagnetic ion cyclotron wave modeling during the geospace environment modeling challenge event. *Journal of Geophysical Research: Space Physics*, *119*, 2963–2977. https://doi.org/10.1002/2013JA019595

Chen, L., Thorne, R. M., Jordanova, V. K., & Horne, R. B. (2010). Global simulation of magnetosonic wave instability in the storm time magnetosphere. *Journal of Geophysical Research*, *115*, A11222. https://doi.org/10.1029/2010JA015707

Chen, L., Thorne, R. M., Jordanova, V. K., Wang, C. P., Gkioulidou, M., Lyons, L., & Horne, R. B. (2010). Global simulation of EMIC wave excitation during the 21 April 2001 storm from coupled RCM-RAM-HOTRAY modeling. *Journal of Geophysical Research*, *115*, A07209. https://doi.org/10.1029/2009JA015075

Cho, J. H., Lee, D. Y., Noh, S. J., Kim, H., Choi, C. R., Lee, J., & Hwang, J. (2017). Spatial dependence of electromagnetic ion cyclotron waves triggered by solar wind dynamic pressure enhancements. *Journal of Geophysical Research: Space Physics*, *122*, 5502–5518. https://doi.org/10.1002/2016JA023827

Colburn, D. S., & Sonett, C. P. (1966). Discontinuities in the solar wind. *Space Science Reviews*, *5*(4), 439–506. https://doi.org/10.1007/BF00240575

Cornwall, J. M. (1965). Cyclotron instabilities and electromagnetic emission in the ultra low frequency and very low frequency ranges. *Journal of Geophysical Research*, *70*(1), 61–69. https://doi.org/10.1029/JZ070i001p00061

Cornwall, J. M., Coroniti, F. V., & Thorne, R. M. (1970). Turbulent loss of ring current protons. *Journal of Geophysical Research*, *75*, 4699–4709. https://doi.org/10.1029/JA075i025p04699

Dalin, P. A., Zastenker, G. N., Paularena, K. I., & Richardson, J. D. (2002). A survey of large, rapid solar wind dynamic pressure changes observed by Interball-1 and IMP 8. *Annales Geophysicae*, *20*(3), 293–299. https://doi.org/10.5194/angeo-20-293-2002

Denton, R. E., Ofman, L., Shprits, Y. Y., Bortnik, J., Millan, R. M., Rodger, C. J., et al. (2019). Pitch angle scattering of sub-MeV relativistic electrons by electromagnetic ion cyclotron waves. *Journal of Geophysical Research: Space Physics*, *124*, 5610–5626. https://doi.org/10.1029/2018JA026384

Engebretson, M. J., Peterson, W. K., Posch, J. L., Klatt, M. R., Anderson, B. J., Russell, C. T., et al. (2002). Observations of two types of Pc1–2 pulsations in the outer dayside magnetosphere. *Journal of Geophysical Research*, *107*(A12), 1451. https://doi.org/10.1029/2001JA000198

Engebretson, M. J., Posch, J. L., Wygant, J. R., Kletzing, C. A., Lessard, M. R., Huang, C. L., et al. (2015). Van Allen probes, NOAA, GOES, and ground observations of an intense EMIC wave event extending over 12 h in magnetic local time. *Journal of Geophysical Research: Space Physics*, *120*, 5465–5488. https://doi.org/10.1002/2015JA021227

Erlandson, R. E., Anderson, B. J., & Zanetti, L. J. (1992). Viking magnetic and electric field observations of periodic Pc1 waves: Pearl pulsations. *Journal of Geophysical Research*, *97*(A10), 14,823–14,832. https://doi.org/10.1029/92JA00838

Fok, M. C., Moore, T. E., & Delcourt, D. C. (1999). Modeling of inner plasma sheet and ring current during substorms. *Journal of Geophysical Research*, *104*(A7), 14,557–14,570. https://doi.org/10.1029/1999JA900014

Fraser, B. J., Grew, R. S., Morley, S. K., Green, J. C., Singer, H. J., Loto'aniu, T. M., & Thomsen, M. F. (2010). Storm time observations of electromagnetic ion cyclotron waves at geosynchronous orbit: GOES results. *Journal of Geophysical Research*, *115*, A05208. https://doi.org/10.1029/2009JA014516

Fraser, B. J., & McPherron, R. L. (1982). Pc1–2 magnetic pulsation spectra and heavy ion effects at synchronous orbit: ATS 6 results. *Journal of Geophysical Research*, *87*(A6), 4560–4566. https://doi.org/10.1029/JA087iA06p04560

Fraser, B., Morley, S., Grew, R., & Singer, H. (2013). Classification of Pc1-2 Electromagnetic Ion Cyclotron Waves at Geosynchronous Orbit. In D. Summers, I. R. Mann, D. N. Baker, & M. Schulz (Eds.), *Dynamics of the Earth's radiation belts and inner magnetosphere*. https://doi.org/10.1029/2012GM001353

Funsten, H. O., Skoug, R. M., Guthrie, A. A., MacDonald, E. A., Baldonado, J. R., Harper, R. W., et al. (2013). Helium, Oxygen, Proton, and Electron (HOPE) mass spectrometer for the Radiation Belt Storm Probes Mission. *Space Science Reviews*, *179*, 423–484. https://doi.org/10.1007/s11214-013-9968-7

Goldstein, J., de Pascuale, S., Kletzing, C., Kurth, W., Genestreti, K. J., Skoug, R. M., et al. (2014). Simulation of Van Allen Probes plasmapause encounters. *Journal of Geophysical Research: Space Physics*, *119*, 7464–7484. https://doi.org/10.1002/2014JA020252

Gosling, J. T., & Pizzo, V. J. (1999). Formation and evolution of corotating interaction regions and their three dimensional structure. *Space Science Reviews*, *89*, 21–52. https://doi.org/10.1023/A:1005291711900

Halford, A. J., Fraser, B. J., & Morley, S. K. (2015). EMIC waves and plasmaspheric and plume density: CRRES results. *Journal of Geophysical Research: Space Physics*, *120*, 1974–1992. https://doi.org/10.1002/2014JA020338

Halford, A. J., Fraser, B. J., Morley, S. K., Elkington, S. R., & Chan, A. A. (2016). Dependence of EMIC wave parameters during quiet, geomagnetic storm, and geomagnetic storm phase times. *Journal of Geophysical Research: Space Physics*, *121*, 6277–6291. https://doi.org/10.1002/2016JA022694

Harang, L. (1936). Oscillations and vibrations in magnetic records at high-latitude stations. *Terrestrial Magnetism and Atmospheric Electricity*, *41*(4), 329. https://doi.org/10.1029/TE041i004p00329

Hirasawa, T. (1981). Effects of magnetospheric compression and expansion on spectral structure of ULF emissions. *Memoirs of National Institute of Polar Research*, *18*, 127–151.

Horne, R. B., & Thorne, R. M. (1993). On the preferred source location for the convective amplification of ion cyclotron waves. *Journal of Geophysical Research*, *98*, 9233–9247. https://doi.org/10.1029/92JA02972

Hudson, P. D. (1970). Discontinuities in an anisotropic plasma and their identification in the solar wind. *Planetary and Space Science*, *18*(11), 1611–1622. https://doi.org/10.1016/0032-0633(70)90036-X

Hudson, P. D. (1971). Rotational discontinuities in an anisotropic plasma. *Planetary and Space Science*, *19*(12), 1693–1699. https://doi.org/10.1016/0032-0633(71)90129-2

Hudson, P. D. (1973). Rotational discontinuities in an anisotropic plasma—II. *Planetary and Space Science*, *21*(3), 475–483. https://doi.org/10.1016/0032-0633(73)90044-5

Jordanova, V. K., Albert, J., & Miyoshi, Y. (2008). Relativistic electron precipitation by EMIC waves from self-consistent global simulations. *Journal of Geophysical Research*, *113*, A00A10. https://doi.org/10.1029/2008JA013239

Jordanova, V. K., Farrugia, C. J., Thorne, R. M., Khazanov, G. V., Reeves, G. D., & Thomsen, M. F. (2001). Modeling ring current proton precipitation by electromagnetic ion cyclotron waves during the May 14–16, 1997, storm. *Journal of Geophysical Research*, *106*, 7–22. https://doi.org/10.1029/2000JA002008

Jun, C. W., Yue, C., Bortnik, J., Lyons, L. R., Nishimura, Y., Kletzing, C., et al. (2019). A statistical study of EMIC waves associated with and without energetic particle injection from the magnetotail. *Journal of Geophysical Research: Space Physics*, *124*, 433–450. https://doi.org/10.1029/2018JA025886

Kangas, J., Aikio, A., & Olson, J. V. (1986). Multistation correlation of ULF pulsation spectra associated with sudden impulses. *Planetary and Space Science*, *34*(6), 543–553. https://doi.org/10.1016/0032-0633(86)90092-9

Kennel, C. (1966). Low-frequency whistler mode. *Physics of Fluids*, *9*, 2190–2202. https://doi.org/10.1063/1.1761588

Kennel, C. F., & Petschek, H. E. (1966). Limit on stably trapped particle fluxes. *Journal of Geophysical Research*, *71*, 1–28. https://doi.org/10.1029/JZ071i001p00001

Khazanov, G. V., Gamayunov, K. V., Gallagher, D. L., & Kozyra, J. U. (2006). Self-consistent model of magnetospheric ring current and propagating electromagnetic ion cyclotron waves: Waves in multi-ion magnetosphere. *Journal of Geophysical Research*, *111*, A10202. https://doi.org/10.1029/2006JA011833

Kletzing, C. A., Kurth, W. S., Acuna, M., MacDowall, R. J., Torbert, R. B., Averkamp, T., et al. (2013). The Electric and Magnetic Field Instrument Suite and Integrated Science (EMFISIS) on RBSP. *Space Science Reviews*, *179*, 127–181. https://doi.org/10.1007/s11214-013-9993-6

Koval, A., & Szabo, A. (2013). Magnetic field turbulence spectra observed by the wind spacecraft. *AIP Conference Proceedings*, *1539*(1), 211–214. https://doi.org/10.1063/1.4811025

Kurth, W. S., Pascuale, S. D., Faden, J. B., Kletzing, C. A., Hospodarsky, G. B., Thaller, S., & Wygant, J. R. (2014). Electron densities inferred from plasma wave spectra obtained by the waves instrument on Van Allen Probes. *Journal of Geophysical Research: Space Physics*, *120*, 904–914. https://doi.org/10.1002/2014JA020857

Landau, L., & Lifshitz, E. (1984). Magnetohydrodynamics. In *Electrodynamics of continuous media*, Course of Theoretical Physics (Vol. 8, Chap. 2, pp. 225–256). Amsterdam: Pergamon. https://doi.org/10.1016/B978-0-08-030275-1.50014-X

Lee, K. H. (2017). Generation of parallel and quasi-perpendicular EMIC waves and mirror waves by fast magnetosonic shocks in the solar wind. *Journal of Geophysical Research: Space Physics*, *122*, 7307–7322. https://doi.org/10.1002/2017JA024340

Li, W., Shprits, Y. Y., & Thorne, R. M. (2007). Dynamic evolution of energetic outer zone electrons due to wave-particle interactions during storms. *Journal of Geophysical Research*, *112*, A10220. https://doi.org/10.1029/2007JA012368

Li, W., Thorne, R. M., Bortnik, J., Nishimura, Y., Angelopoulos, V., Chen, L., et al. (2010). Global distributions of suprathermal electrons observed on THEMIS and potential mechanisms for access into the plasmasphere. *Journal of Geophysical Research*, *115*, A00J10. https://doi.org/10.1029/2010JA015687

Li, L. Y., Yu, J., Cao, J. B., & Yuan, Z. G. (2016). Compression-amplified EMIC waves and their effects on relativistic electrons. *Physics of Plasmas*, *23*(6), 062116. https://doi.org/10.1063/1.4953899

Lin, R. P., Anderson, K. A., Ashford, S., Carlson, C., Curtis, D., Ergun, R., et al. (1995). A three-dimensional plasma and energetic particle investigation for the wind spacecraft. *Space Science Reviews*, *71*(1–4), 125–153. https://doi.org/10.1007/BF00751328

Liu, N., Su, Z., Gao, Z., Zheng, H., Wang, Y., Wang, S., et al. (2017). Simultaneous disappearances of plasmaspheric hiss, exohiss, and chorus waves triggered by a sudden decrease in solar wind dynamic pressure. *Geophysical Research Letters*, *44*, 52–61. https://doi.org/10.1002/2016GL071987

Liu, N., Su, Z., Zheng, H., Wang, Y., & Wang, S. (2018a). Magnetosonic harmonic falling and rising frequency emissions potentially generated by nonlinear wave-wave interactions in the Van Allen Radiation Belts. *Geophysical Research Letters*, *45*, 7985–7995. https://doi.org/10.1029/2018GL079232

Liu, N., Su, Z., Zheng, H., Wang, Y., & Wang, S. (2018b). Prompt disappearance and emergence of radiation belt magnetosonic waves induced by solar wind dynamic pressure variations. *Geophysical Research Letters*, *45*, 585–594. https://doi.org/10.1002/2017GL076382

Loto'Aniu, T. M., Fraser, B. J., & Waters, C. L. (2005). Propagation of electromagnetic ion cyclotron wave energy in the magnetosphere. *Journal of Geophysical Research*, *110*, A07214. https://doi.org/10.1029/2004JA010816

Lyons, L. R., & Thorne, R. M. (1972). Parasitic pitch angle diffusion of radiation belt particles by ion cyclotron waves. *Journal of Geophysical Research*, *77*, 5608.

Mauk, B. H., Fox, N. J., Kanekal, S. G., Kessel, R. L., Sibeck, D. G., & Ukhorskiy, A. (2013). Science objectives and rationale for the Radiation Belt Storm Probes mission. *Space Science Reviews*, *179*, 3–27. https://doi.org/10.1007/s11214-012-9908-y

McCollough, J. P., Elkington, S. R., & Baker, D. N. (2009). Modeling EMIC wave growth during the compression event of 29 June 2007. *Geophysical Research Letters*, *36*, L18108. https://doi.org/10.1029/2009GL039985

McCollough, J. P., Elkington, S. R., & Baker, D. N. (2012). The role of Shabansky orbits in compression-related electromagnetic ion cyclotron wave growth. *Journal of Geophysical Research*, *117*, A01208. https://doi.org/10.1029/2011JA016948

McFadden, J. P., Carlson, C. W., Larson, D., Bonnell, J., Mozer, F., Angelopoulos, V., et al. (2008). THEMIS ESA first science results and performance issues. *Space Science Reviews*, *141*, 477–508. https://doi.org/10.1007/s11214-008-9433-1

Mitchell, D. G., Lanzerotti, L. J., Kim, C. K., Stokes, M., Ho, G., Cooper, S., et al. (2013). Radiation Belt Storm Probes Ion Composition Experiment (RBSPICE). *Space Science Reviews*, *179*, 263–308. https://doi.org/10.1007/s11214-013-9965-x

Nakamura, S., Omura, Y., & Angelopoulos, V. (2016). A statistical study of EMIC rising and falling tone emissions observed by THEMIS. *Journal of Geophysical Research: Space Physics*, *121*, 8374–8391. https://doi.org/10.1002/2016JA022353

Neugebauer, M. (2006). Comment on the abundances of rotational and tangential discontinuities in the solar wind. *Journal of Geophysical Research*, *111*, A04103. https://doi.org/10.1029/2005JA011497

Ogilvie, K. W., Chornay, D. J., Fritzenreiter, R. J., Hunsaker, F., Keller, J., Lobell, J., et al. (1995). SWE, a comprehensive plasma instrument for the wind spacecraft. *Space Science Reviews*, *71*(1–4), 55–77. https://doi.org/10.1007/BF00751326

Ogilvie, K., & Desch, M. (1997). The WIND spacecraft and its early scientific results. *Advances in Space Research*, *20*, 559–568.

Olson, J. V., & Lee, L. C. (1983). Pc1 wave generation by sudden impulses. *Planet Space Science*, *31*(3), 295–302. https://doi.org/10.1016/0032-0633(83)90079-X

Omura, Y., Pickett, J., Grison, B., Santolik, O., Dandouras, I., Engebretson, M., et al. (2010). Theory and observation of electromagnetic ion cyclotron triggered emissions in the magnetosphere. *Journal of Geophysical Research*, *115*, A07234. https://doi.org/10.1029/2010JA015300

Omura, Y., & Zhao, Q. (2012). Nonlinear pitch-angle scattering of relativistic electrons by EMIC waves in the inner magnetosphere. *Journal of Geophysical Research*, *117*, A08227. https://doi.org/10.1029/2012JA017943

Perraut, S. (1982). Wave-particle interactions in the ULF range: GEOS-1 and -2 results. *Planetary and Space Science*, *30*(12), 1219–1227. https://doi.org/10.1016/0032-0633(82)90095-2

Pickett, J. S., Grison, B., Omura, Y., Engebretson, M. J., Dandouras, I., Masson, A., et al. (2010). Cluster observations of EMIC triggered emissions in association with Pc1 waves near Earth's plasmapause. *Geophysical Research Letters*, *37*, 9104. https://doi.org/10.1029/2010GL042648

Rauch, J. L., & Roux, A. (1982). Ray tracing of ULF waves in a multicomponent magnetospheric plasma: Consequences for the generation mechanism of ion cyclotron waves. *Journal of Geophysical Research*, *87*(A10), 8191–8198. https://doi.org/10.1029/JA087iA10p08191

Remya, B., Sibeck, D. G., Halford, A. J., Murphy, K. R., Reeves, G. D., Singer, H. J., et al. (2018). Ion injection triggered EMIC waves in the Earth's magnetosphere. *Journal of Geophysical Research: Space Physics*, *123*, 4921–4938. https://doi.org/10.1029/2018JA025354

Remya, B., Sibeck, D. G., Ruohoniemi, J. M., Kunduri, B., Halford, A. J., Reeves, G. D., & Reddy, R. V. (2020). Association Between EMIC wave occurrence and enhanced convection periods during ion injections. *Geophysical Research Letters*, *47*, e2019GL085676. https://doi.org/10.1029/2019GL085676

Riazantseva, M. O., Khabarova, O. V., Zastenker, G. N., & Richardson, J. D. (2007). Sharp boundaries of solar wind plasma structures and their relationship to solar wind turbulence. *Advances in Space Research*, *40*(12), 1802–1806. https://doi.org/10.1016/j.asr.2007.05.004

Saikin, A. A., Zhang, J. C., Smith, C. W., Spence, H. E., Torbert, R. B., & Kletzing, C. A. (2016). The dependence on geomagnetic conditions and solar wind dynamic pressure of the spatial distributions of EMIC waves observed by the Van Allen Probes. *Journal of Geophysical Research: Space Physics*, *121*, 4362–4377. https://doi.org/10.1002/2016JA022523

Santolík, O., Parrot, M., & Lefeuvre, F. (2003). Singular value decomposition methods for wave propagation analysis. *Radio Science*, *38*(1), 1010. https://doi.org/10.1029/2000RS002523

Santolík, O., Pickett, J. S., Gurnett, D. A., Menietti, J. D., Tsurutani, B. T., & Verkhoglyadova, O. (2010). Survey of Poynting flux of whistler mode chorus in the outer zone. *Journal of Geophysical Research*, *115*, A00F13. https://doi.org/10.1029/2009JA014925

Santolík, O., Pickett, J. S., Gurnett, D. A., & Storey, L. R. O. (2002). Magnetic component of narrowband ion cyclotron waves in the auroral zone. *Journal of Geophysical Research*, *107*, 1444. https://doi.org/10.1029/2001JA000146

Sarno-Smith, L. K., Larsen, B. A., Skoug, R. M., Liemohn, M. W., Breneman, A., Wygant, J. R., & Thomsen, M. F. (2016). Spacecraft surface charging within geosynchronous orbit observed by the Van Allen Probes. *Space Weather*, *14*, 151–164. https://doi.org/10.1002/2015SW001345

Shprits, Y. Y., Drozdov, A. Y., Spasojevic, M., Kellerman, A. C., Usanova, M. E., Engebretson, M. J., et al. (2016). Wave-induced loss of ultra-relativistic electrons in the Van Allen radiation belts. *Nature Communications*, *7*, 12883. https://doi.org/10.1038/ncomms12883

Sibeck, D. G., McEntire, R. W., Lui, A. T. Y., Lopez, R. E., & Krimigis, S. M. (1987). Magnetic field drift shell splitting: Cause of unusual dayside particle pitch angle distributions during storms and substorms. *Journal of Geophysical Research*, *92*(A12), 13,485–13,497. https://doi.org/10.1029/JA092iA12p13485

Smith, E. J. (1973). Identification of interplanetary tangential and rotational discontinuities. *Journal of Geophysical Research*, *78*(13), 2054. https://doi.org/10.1029/JA078i013p02054

Smith, E. J., & Wolfe, J. H. (1976). Observations of interaction regions and corotating shocks between one and five AU: Pioneers 10 and 11. *Geophysical Research Letters*, *3*(3), 137–140. https://doi.org/10.1029/GL003i003p00137

Sonnerup, B. U. O., & Cahill, J. (1967). Magnetopause structure and attitude from explorer 12 observations. *Journal of Geophysical Research*, *72*, 171. https://doi.org/10.1029/JZ072i001p00171

Spence, H. E., Reeves, G. D., Baker, D. N., Blake, J. B., Bolton, M., Bourdarie, S., et al. (2013). Science goals and overview of the energetic particle, composition, and thermal plasma (ECT) Suite on NASA's Radiation Belt Storm Probes (RBSP) Mission. *Space Science Reviews*, *179*, 311–336. https://doi.org/10.1007/s11214-013-0007-5

Stix, T. H. (1962). *The theory of plasma waves*. New York: McGraw-Hill.

Su, Z., Liu, N., Zheng, H., Wang, Y., & Wang, S. (2018). Large-amplitude extremely low frequency hiss waves in plasmaspheric plumes. *Geophysical Research Letters*, *45*, 565–577. https://doi.org/10.1002/2017GL076754

Su, Z., Xiao, F., Zheng, H., & Wang, S. (2011). CRRES observation and STEERB simulation of the 9 October 1990 electron radiation belt dropout event. *Geophysical Research Letters*, *38*, L06106. https://doi.org/10.1029/2011GL046873

Sucksdorff, E. (1936). Occurrences of rapid micropulsations at Sodankylä during 1932 to 1935. *Terrestrial Magnetism and Atmospheric Electricity*, *41*(4), 337. https://doi.org/10.1029/TE041i004p00337

Summers, D., Ni, B., & Meredith, N. P. (2007). Timescales for radiation belt electron acceleration and loss due to resonant wave-particle interactions: 1. Theory. *Journal of Geophysical Research*, *112*, A04206. https://doi.org/10.1029/2006JA011801

Summers, D., & Thorne, R. M. (2003). Relativistic electron pitch-angle scattering by electromagnetic ion cyclotron waves during geomagnetic storms. *Journal of Geophysical Research*, *108*(A4), 1143. https://doi.org/10.1029/2002JA009489

Takahashi, K., Anderson, B. J., Ohtani, S. i., Reeves, G. D., Takahashi, S., Sarris, T. E., & Mursula, K. (1997). Drift-shell splitting of energetic ions injected at pseudo-substorm onsets. *Journal of Geophysical Research*, *102*(A10), 22,117–22,130. https://doi.org/10.1029/97JA01870

Thorne, R. M., & Horne, R. B. (1992). The contribution of ion-cyclotron waves to electron heating and SAR-arc excitation near the storm-time plasmapause. *Geophysical Research Letters*, *19*(4), 417–420. https://doi.org/10.1029/92GL00089

Thorne, R. M., & Horne, R. B. (1994). Energy transfer between energetic ring current H^+ and O^+ by electromagnetic ion cyclotron waves. *Journal of Geophysical Research*, *99*, 17275. https://doi.org/10.1029/94JA01007

Thorne, R. M., & Kennel, C. F. (1971). Relativistic electron precipitation during magnetic storm main phase. *Journal of Geophysical Research*, *76*, 4446–4453. https://doi.org/10.1029/JA076i019p04446

Troitskaya, V. A. (1967). Micropulsations and the State of the Magnetosphere. In J. W. King & W. S. Newman (Eds.), *Solar-terrestrial physics* (pp. 213–274). New York: Academic Press.

Tsyganenko, N. A., & Andreeva, V. A. (2015). A forecasting model of the magnetosphere driven by an optimal solar wind coupling function. *Journal of Geophysical Research: Space Physics*, *120*, 8401–8425. https://doi.org/10.1002/2015JA021641

Usanova, M. E., Drozdov, A., Orlova, K., Mann, I. R., Shprits, Y., Robertson, M. T., et al. (2014). Effect of EMIC waves on relativistic and ultrarelativistic electron populations: Ground-based and Van Allen Probes observations. *Geophysical Research Letters*, *41*, 1375–1381. https://doi.org/10.1002/2013GL059024

Usanova, M. E., Mann, I. R., Bortnik, J., Shao, L., & Angelopoulos, V. (2012). THEMIS observations of electromagnetic ion cyclotron wave occurrence: Dependence on AE, SYMH, and solar wind dynamic pressure. *Journal of Geophysical Research*, *117*, A10218. https://doi.org/10.1029/2012JA018049

Usanova, M. E., Mann, I. R., Rae, I. J., Kale, Z. C., Angelopoulos, V., Bonnell, J. W., et al. (2008). Multipoint observations of magnetospheric compression-related EMIC Pc1 waves by THEMIS and CARISMA. *Geophysical Research Letters*, *35*, L17S25. https://doi.org/10.1029/2008GL034458

Wang, D., Yuan, Z., Yu, X., Deng, X., Zhou, M., Huang, S., et al. (2015). Statistical characteristics of EMIC waves: Van Allen Probe observations. *Journal of Geophysical Research: Space Physics*, *120*, 4400–4408. https://doi.org/10.1002/2015JA021089

Wu, B. H., Mandt, M. E., Lee, L. C., & Chao, J. K. (1993). Magnetospheric response to solar wind dynamic pressure variations: Interaction of interplanetary tangential discontinuities with the bow shock. *Journal of Geophysical Research*, *98*(A12), 21,297–21,312. https://doi.org/10.1029/93JA01013

Wygant, J., Bonnell, J., Goetz, K., Ergun, R., Mozer, F., Bale, S., et al. (2013). The electric field and waves instruments on the Radiation Belt Storm Probes mission. *Space Science Reviews*, *179*(1–4), 183–220. https://doi.org/10.1007/s11214-013-0013-7

Yuan, Z., Xiong, Y., Huang, S., Deng, X., Pang, Y., Zhou, M., et al. (2014). Cold electron heating by EMIC waves in the plasmaspheric plume with observations of the Cluster satellite. *Geophysical Research Letters*, *41*, 1830–1837. https://doi.org/10.1002/2014GL059241

Yue, C., Bortnik, J., Thorne, R. M., Ma, Q., An, X., Chappell, C. R., et al. (2017). The characteristic pitch angle distributions of 1 eV to 600 keV protons near the equator based on Van Allen Probes observations. *Journal of Geophysical Research: Space Physics*, *122*, 9464–9473. https://doi.org/10.1002/2017JA024421

Zhang, X. J., Li, W., Thorne, R. M., Angelopoulos, V., Bortnik, J., Kletzing, C. A., et al. (2016). Statistical distribution of EMIC wave spectra: Observations from Van Allen Probes. *Geophysical Research Letters*, *43*, 12,348–12,355. https://doi.org/10.1002/2016GL071158

Zhang, Y., Paxton, L. J., & Zheng, Y. (2008). Interplanetary shock induced ring current auroras. *Journal of Geophysical Research*, *113*, A01212. https://doi.org/10.1029/2007JA012554

Zhang, J. C., Saikin, A. A., Kistler, L. M., Smith, C. W., Spence, H. E., Mouikis, C. G., et al. (2014). Excitation of EMIC waves detected by the Van Allen Probes on 28 April 2013. *Geophysical Research Letters*, *41*, 4101–4108. https://doi.org/10.1002/2014GL060621

Zhou, Q., Xiao, F., Yang, C., He, Y., & Tang, L. (2013). Observation and modeling of magnetospheric cold electron heating by electromagnetic ion cyclotron waves. *Journal of Geophysical Research: Space Physics*, *118*, 6907–6914. https://doi.org/10.1002/2013JA019263

Zuo, P., Feng, X., Xie, Y., Wang, Y., Li, H., & Xu, X. (2015). Automatic detection algorithm of dynamic pressure pulses in the solar wind. *Astrophysical Journal*, *803*(2), 94. https://doi.org/10.1088/0004-637X/803/2/94